

# Shakedown and Limit Analysis of 90° Pipe Bends Under Internal Pressure, Cyclic In-plane Bending and Cyclic Thermal Loading

Haofeng Chen\*, James Ure, Tianbai Li, Weihang Chen, Donald Mackenzie

Department of Mechanical Engineering, University of Strathclyde, Glasgow, G1 1XJ

## **Abstract**

The Linear Matching Method is used to create the shakedown limit and limit load interaction curves of 90 degree pipe bends for a range of bend factors. Two load cases are considered i) internal pressure and in-plane bending (which includes opening, closing and reversed bending) and ii) internal pressure and a cyclic through wall temperature difference giving rise to thermal stresses. The effects of the ratios of bend radius to pipe mean radius ( $R/r$ ) and mean radius to wall thickness ( $r/t$ ) on the limit load and shakedown behaviour are presented.

Keywords: Pipe bend, shakedown, limit load, reverse plasticity, ratchetting

## **1. Introduction**

90° pipe bends are common in piping systems, and it is vital to ensure that these components are designed against plastic collapse. Additionally, design against incremental plastic collapse (ratchetting) or low cycle fatigue failure (resulting from alternating plasticity) must also be performed. The conservatism resulting from limiting the structure to purely elastic behaviour is often not acceptable and components are allowed to shakedown, which allows plastic deformation that does not result in either alternating plasticity or ratchetting.

The shakedown of structures has been studied by many researchers. The complexity of the phenomenon means that analytical solutions exist for only the simplest of geometries and loading. Incremental Finite Element Analysis (FEA) can be used to predict if elastic shakedown, alternating plasticity or ratchetting occurs but does not evaluate limits or boundaries between these different responses. Creation of the Bree-like [1] shakedown boundary diagrams requires many FEA calculations to be performed, which becomes very computationally expensive with complex geometries. Consequently, many direct methods have been created based upon the Koiter [2] kinematic and Melan [3] static theorems to calculate the shakedown limit. Typical of these are the GLOSS R-node method [4], the Elastic Compensation Method [5], mathematical programming methods [6] and the Linear Matching Method (LMM) [7,8]. The LMM has been shown to give accurate results for many geometries with complex load histories and temperature dependent

material properties. LMM ABAQUS subroutines have been consolidated by the British Energy Generation Ltd R5 research program and are used in the assessment of plant components [9].

The LMM is used in this work to analyse the shakedown behaviour of 90 degree pipe bends. First a summary of current literature regarding the shakedown of this geometry is given, followed by an explanation of the LMM procedure, the Finite Element model used and finally the results, discussion and conclusions.

## **2. Summary of Limit and Shakedown Analysis of Pipe Bends**

Figure 1 shows a typical 90° pipe bend. Such bends are commonly described in terms of two ratios:  $r/t$  and  $R/r$ , where  $r$  is the mean pipe radius,  $R$  is the bend radius and  $t$  is the wall thickness. When these ratios are combined, they give the bend characteristic of the pipe,  $h$ :

$$h = \frac{R/r}{r/t} = \frac{Rt}{r^2} \quad (1)$$

### **2.1 Limit Load Solutions**

Considerable attention has been given to limit analysis of pipe bends under in-plane bending and internal pressure in recent years. Calladine [10] derived a limit moment equation for pipe bends with no attached straight sections using thin shell theory:

$$M_L = 1.19\pi^2 t \sigma_y h^{2/3} \quad \text{where } h \leq 0.5 \quad (2)$$

where  $\sigma_y$  is the yield stress of the material. Goodall [11] derived a limit pressure expression for bends with no attached straights, also using thin shell theory and the Tresca yield criterion:

$$P_L = \sigma_y \frac{t}{r} \frac{\left(1 - \frac{r}{R}\right)}{\left(1 - \frac{r}{2R}\right)} \quad (3)$$

Other than these equations, no further theoretical solutions could be found for the plastic limit of this geometry. Instead, researchers have used extensive FEA to generate data for various ratios of  $R/r$  and  $r/t$ . These data points have then been plotted and equations derived from curve-fits of the data. A recent review of the literature by Lei [12] has highlighted some important conclusions. Firstly, the attached straight sections provide a significant level of reinforcement to the bend by

allowing the plastic zone to spread. This increases the limit loads above those calculated by Calladine and Goodall. The literature presents many equations for the limit load of a pipe bend under in-plane bending, internal pressure and combination loading based on both small and large deformation FEA.

Whilst these equations provide a good fit to the data they are derived from, it is found that in many cases the equations do not successfully predict the results from other authors, especially when combined loading is concerned. Additionally, the range of pipe bend characteristics which these equations describe are too narrow to be applied to the range analysed in this work (a general maximum found was  $h = 0.7$  compared to  $h = 1$  in this paper). As a result of this, as well as the fact that the geometries with  $r/t = 5$  cannot be considered "thin" as an approximation, the results presented here are normalised against the limit pressure and moment for a thick walled straight pipe with the same mean radius and wall thickness:

$$P_L^s = \frac{2}{\sqrt{3}} \sigma_y \ln\left(\frac{r_o}{r_i}\right) \quad (4)$$

$$M_L^s = \frac{4}{3} \sigma_y (r_o^3 - r_i^3) \quad (5)$$

where  $r_o$  and  $r_i$  are the outer and inner radii of the pipe respectively. All limit analyses in the literature concerns mechanical loading only as thermal loading and thermal stresses have no effect on the limit load of a component.

## 2.2 Shakedown Analysis

Despite the extensive volume of work regarding limit analysis and limit load solutions for mechanical loading, very little work has been published regarding the shakedown behaviour of this geometry. H.F. Abdalla et al [13] presented the shakedown behaviour of a single bend with  $R = 480\text{mm}$ ,  $r = 133.5\text{mm}$  and  $t = 3\text{mm}$  (giving  $R/r = 3.6$  and  $r/t = 44.5$ ).

Further calculations are carried out by C.S Oh et al [14] for the shakedown of bends covering a large range of  $h$  for internal pressure and in-plane closing and opening bending (reversed bending and thermal loading is not considered). In [14], the same lower bound numerical technique is used as in [13], which is thought by the authors of this work to give solutions which are too conservative when compared to the exact shakedown limit solution.

Unlike limit analysis, cyclic thermal loading may play an important role in the shakedown limits, however, no published work could be found regarding the shakedown of pipe bends under thermal and mechanical loading.

The objective of this paper is to use the Linear Matching Method to analyse the shakedown and limit loads of 90° pipe bends subject to both mechanical and thermal loading in a systematic manner. Two cases are considered. The first is when the pipe is subjected to an internal pressure and in-plane closing, opening and reversed bending. The mechanisms of reverse plasticity and ratchetting are explored and a comparison between the shakedown behaviour of opening, closing and reversed bending is presented. The second case is where the pipe is subjected to an internal pressure and a cyclic temperature gradient through the wall thickness. The effect of temperature dependent yield stress is considered and the shakedown behaviour of pipe bends is compared to that of a straight pipe. Although large deformation calculations introduces geometric strengthening and weakening effects, which for pipe bends takes the form of the ovalisation of the section due to the applied moment, small deformation analysis is shown to give consistent and conservative results. Therefore small deformation assumptions are used throughout.

### **3. Overview of LMM**

The Linear Matching Method has been described in detail in other works [7,8]. A basic overview is presented here for convenience.

The basis of the Linear Matching Method is that limit state solutions can be developed by systematically reducing the modulus in regions of high stress of a linear elastic solution. Doing so reduces the maximum stress in these regions and allows the stress to re-distribute in the body, which in turn increases the load at which all stresses lie within yield. The material is assumed to be linear elastic-perfectly plastic and to satisfy both the von-Mises yield criterion and the plastic incompressibility condition.

An iteration of this procedure begins with calculation of the new shear modulus  $\mu$  based upon the stress from the previous linear solution and the strain rate  $\dot{\bar{\epsilon}}^i$ , given by

$$\mu = \frac{2\sigma_y}{3\dot{\bar{\epsilon}}^i} \quad (6)$$

where  $\sigma_y$  is the yield stress of the material. Consider a body of volume  $V$ , with surface area,  $S$ . The body is subjected to mechanical loads  $\lambda P(x,t)$ , and a thermal loads  $\lambda\theta(x,t)$  which are applied over a part of the surface  $S_T$ . The remainder of the surface area is constrained to have zero displacement rate  $\dot{u}_i = 0$ . These loads are applied over the time cycle  $0 \leq t \leq \Delta t$ . The linear elastic stress solution  $\lambda\hat{\sigma}_{ij}$ , is calculated from these loads as

$$\lambda \hat{\sigma}_{ij}(x_i, t) = \lambda \hat{\sigma}_{ij}^{\theta}(x_i, t) + \lambda \hat{\sigma}_{ij}^p(x_i, t) \quad (7)$$

where  $\lambda \hat{\sigma}_{ij}^{\theta}$  and  $\lambda \hat{\sigma}_{ij}^p$  are the elastic solutions corresponding to  $\lambda \theta(x, t)$  and  $\lambda P(x, t)$  respectively.  $\lambda$  is introduced as a load parameter so that a range of loading histories can be considered. For cyclic loading, the stress history over the time cycle  $0 \leq t \leq \Delta t$  is given by

$$\sigma_{ij} = \lambda \hat{\sigma}_{ij}(x_i, t) + \bar{\rho}_{ij}(x_i) + \rho_{ij}^r(x_i, t) \quad (8)$$

where  $\bar{\rho}_{ij}(x_i)$  is the self-equilibrating constant residual stress field and corresponds to the residual state of stress at the beginning and end of each cycle.  $\rho_{ij}^r(x_i, t)$  denotes the changing component of residual stress through the cycle, which for shakedown conditions must equal zero, meaning that the cyclic stress history at shakedown is given by

$$\sigma_{ij} = \lambda \hat{\sigma}_{ij}(x_i, t) + \bar{\rho}_{ij}(x_i) \quad (9)$$

Based on Koiter's theorem [2], the upper bound shakedown limit,  $\lambda_{UB}$  is given by:

$$\lambda_{UB} = \frac{\int_V \int_0^{\Delta t} \sigma_v \bar{\dot{\epsilon}}(\dot{\epsilon}_{ij}) dt dV}{\int_V \int_0^{\Delta t} (\hat{\sigma}_{ij} \dot{\epsilon}_{ij}) dt dV} \quad (10)$$

where  $\dot{\epsilon}_{ij}$  is a kinematically admissible strain rate and  $\bar{\dot{\epsilon}} = \sqrt{\frac{2}{3} \dot{\epsilon}_{ij} \dot{\epsilon}_{ij}}$  is the effective strain rate. Consecutive iterations of the procedure is shown to converge to the least upper bound,  $\lambda_{UB} \geq \lambda_s$  where  $\lambda_s$  is the exact shakedown multiplier. The lower bound is found by Melan's theorem [3], which states that the structure will shakedown if the superposition of the applied stresses and residual stresses do not violate the temperature dependent yield condition at any point:

$$f(\lambda_{LB} \hat{\sigma}_{ij}(x_i, t) + \bar{\rho}_{ij}(x_i)) \leq 0 \quad (11)$$

where  $\lambda_{LB}$  is the lower bound shakedown multiplier.

This procedure can be implemented in the commercial finite element software package ABAQUS [15] through the use of the user subroutine UMAT. In each iteration, the linear problem is solved for stress, strain and displacement. The UMAT subroutine computes the varying shear modulus, the Jacobian matrix, the residual stress and the updated stress for a given strain increment. The upper bound shakedown limit is found by integrating equation (10) over the entire volume and this is used

in the next iteration. The lower bound shakedown multiplier is found by checking the condition for all integration points.

Shakedown analysis deals with cyclic load conditions, which may have any number of load extremes over the time cycle. Hence, the limit load can be determined using the procedure described above as a special case of shakedown, where the number of load extremes in the cyclic load domain reduces to one; i.e. a monotonic load condition.

#### **4. FEA Model**

A three dimensional solid model was constructed in ABAQUS. Due to the symmetry of the geometry, a one quarter model was used and symmetry boundary conditions were applied (see Figure 2). ABAQUS type C3D20R quadratic elements with reduced integration were used for the structural analysis and ABAQUS type DC3D20 elements were used for the heat transfer analysis.

To mesh the bend, at least three elements were used through the thickness, ten around the radius of the bend and twenty elements around the circumference of the pipe. A refinement study was conducted to validate the accuracy of the mesh used. Such a mesh was chosen to give sufficient density around the area of interest and to maintain reasonable element aspect ratios. The attached straight section was meshed with twenty elements along its length, which were biased to be smaller in the region of the bend.

The internal pressure,  $P$ , was applied at the inner surface assuming the closed end condition, with an equivalent axial tension applied at the free end of the straight section to replicate the axial stress. The moment was applied as a linear pressure distribution at the free end of the straight section, which was applied using the user subroutine DLOAD in ABAQUS (Figure 3).

When conducting a limit analysis, the pressure and moment loads were applied monotonically. When shakedown analysis was performed, the pressure was held at a constant value and the initial bending moment was cycled i) from zero to a maximum of  $M$  for opening bending ii) from zero to a minimum of  $-M$  for closing bending or iii) from  $-0.5M$  to  $+0.5M$  for reversed bending, shown in Figure 4.

When the case of internal pressure and cyclic thermal loading was considered, a steady state heat transfer analysis was conducted with  $T_o = 100^\circ\text{C}$  applied at the inner surface and  $0^\circ\text{C}$  at the outer surface to construct the most severe thermal history. The temperature distribution calculated by this heat transfer analysis was then applied to the model, which gives rise to initial maximum stresses in a thermal cycle. An additional constraint was added - the free end of the pipe was constrained via

equations to expand in-plane along its length, simulating the thermal expansion of a long pipe. The temperature gradient through the wall thickness was cycled from zero to a maximum and back to zero over the time step.

Analysis of 9 geometries is presented with  $R/r = 2, 3$  and  $5$ , each of which with  $r/t = 5, 10$  and  $20$ , which gives  $0.1 \leq h \leq 1$ . In each case the attached straight sections were a length such that  $L/R = 8$ , which was found to be more than adequate to always provide the maximum reinforcement possible to the bend. In each case a Young's Modulus of  $200\text{GPa}$  and a Poisson's ratio of  $0.3$  was used. The steel is assumed to have a thermal conductivity of  $43\text{ W/m}^2\text{K}$  and a thermal expansion coefficient of  $1 \times 10^{-5}\text{ }^\circ\text{C}^{-1}$ . The yield stress is assumed to be temperature dependent, with data for this taken from PD5500 British Standard for unfired welded pressure vessel design [16], as shown in Table 1.

For each analysis, two linear elastic solutions were performed: one for the internal pressure loading and the second for either the bending moment or thermal loading. These two stress solutions are then used to construct the initial stress states in equation (7) to begin the iterative process to find the upper and lower bound shakedown limit multipliers.

### **5. Internal Pressure and Bending Moment**

Figure 5 shows the two elastic solutions for  $R/r = 2$  and  $r/t = 5$  used to construct the initial stress conditions for the shakedown and limit analysis. The internal pressure causes high stresses at the inner surface of the intrados of the bend. The bending moment causes high stresses at the flank.

Figure 6 presents the shakedown limit and limit load interaction curves for  $R/r = 2$  and  $r/t = 5$  under internal pressure and opening bending. It can be seen that the shakedown boundary follows a classic Bree-like shape whereby the reverse plasticity boundary is a constant value of cyclic bending. The limit load surface calculated by the LMM is shown and this has been verified at 5 points using ABAQUS elastic-plastic incremental analysis (using the Rik's method). The difference between the LMM and ABAQUS limit solutions is less than 1%, providing confidence that the LMM produces accurate results.

The contours of plastic strain resulting from the cyclic loading at points A and B in Figure 6 are shown in Figure 7, which correspond to the reverse plasticity limit and the ratchet limit respectively. The plastic strain corresponding to the reverse plasticity limit is restricted to a very small area at the flank of the pipe, with the strains accumulating at the inner surface. The plastic strains corresponding to the ratchet limit occurs globally at the intrados of the bend, with the strains initiating at the outer surface. The locations of ratchetting strain matches those found by Chen, Gao and Chen in [17], giving further confidence in the accuracy of the method. The reverse plasticity

mechanism occurs mainly due to the location of the peak stress caused by the bending moment. The ratchetting mechanism occurs at the location of peak pressure stress, at the intrados of the bend.

Figure 8 shows a comparison between the results obtained by C.S. Oh et al [14] and the results obtained here for  $R/r=2$ ,  $r/t=10$  subject to internal pressure and cyclic opening bending. The data is normalised against equation (2) and the Goodall limit pressure using the von-Mises criterion (equation (3) multiplied by  $2/\sqrt{3}$ ). The method employed by C. S. Oh et al is a lower bound method and both the lower and upper bounds calculated by the LMM are shown in the Figure. Comparison of the two shakedown curves reveals that they produce comparable reverse plasticity boundaries but that the LMM predicts a significantly larger ratchetting boundary.

In order to verify the accuracy of the LMM, the limit load for pressure loading was calculated using ABAQUS Rik's analysis and two points were chosen (labelled C and D in Figure 8) for full cyclic analysis in ABAQUS. The limit pressure given by the Rik's analysis correlates well with the equivalent value calculated by the LMM, with a difference of less than 1% between the two solutions. The plastic strain histories at the for the cyclic loading at points C and D are shown in Figure 9. The strains in Figure 9 were taken from the position of maximum plastic strain, which was at the inner surface at the intrados of the bend. The plastic strain history of point C shows that shakedown is achieved after approximately 100 cycles. Point D shows classic ratchetting behaviour, with the plastic strain increasing every cycle.

These three points all agree well with the shakedown boundary calculated by the LMM, giving confidence in the accuracy of the results produced by this method. Further benefits of the LMM can be found with the computing time taken to generate the shakedown curves. The time taken for the LMM to generate the point on the ratchetting boundary was less than 10% of that taken for the two analyses for points A and B to complete.

The following sections present results which demonstrate the effect of  $h$ ,  $r/t$  and  $R/r$  on the shakedown limit and limit load surface for both opening and closing bending. The applied pressures and moments are normalised against the limit pressure and moment for an equivalent thick walled straight pipe respectively (equations (4) and (5)) to allow ease of comparison between different geometries. It is clear from Figure 6 that the LMM produces lower and upper bound shakedown limits that converge very close to each other. This is representative of all results obtained and for the remainder of this paper only the upper bound limit will be shown for clarity in the Figures.

### 5.1 Effect of Bend Characteristic $h$

Figure 10 shows the shakedown boundaries for all 9 geometries considered subject to constant internal pressure and cyclic opening bending. A clear trend is seen in which the normalised moment (corresponding to the reverse plasticity limit) increases with  $h$ . Plotting the normalised cyclic moment corresponding to the reverse plasticity limit against  $h$  shows a quadratic relationship, given by equation (12):

$$RP_{\text{Limit}} = -0.6638h^2 + 1.4837h + 0.0732 \quad (12)$$

where  $RP_{\text{Limit}}$  is the cyclic moment corresponding to the reverse plasticity limit normalised against the limit moment of a thick walled straight pipe (equation (5)). Other than this trend, no further correlations can be found with  $h$ : the limit pressure, the pressure at which ratchetting begins and the slopes of the ratchetting boundaries do not show a correlation with  $h$ .

## 5.2 Effect of the ratio $r/t$

Figure 11 shows the shakedown limit and limit load surfaces for fixed  $R/r$  values of 2, 3 and 5, and varying  $r/t$  values for an opening bending moment. The general trend for each geometry considered is similar. As  $r/t$  decreases (i.e. the pipe becomes thicker), the limit load surfaces expand, indicating larger loads to failure. Large increases in the limit moment are seen with decreasing  $r/t$  but comparatively little effect is observed in the normalised limit pressure. The graphs also reveal that the alternating plasticity boundary occurs at higher values of normalised moment with decreasing  $r/t$ .

One interesting observation is the margin between the limit load and the shakedown limit surfaces. In general, there is a significant margin between both lines at low pressures, which reduces to a minimum at around the point where alternating plasticity changes to ratchetting. At pressures larger than this the margin increases once more before converging to the limit load for pressure loading. As  $r/t$  becomes smaller, the margin between the two lines becomes smaller to the extent that there is almost no margin between the shakedown and limit loads for a large normalised pressure range for  $R/r = 3$ ,  $r/t = 5$  and  $R/r = 5$  and  $r/t = 5$ . This phenomenon is particularly important for the designer. The shakedown behaviour for cyclic loading of the bend may, for some loading conditions, be very close to the limit load for monotonic loading. In such cases, the conservatism in the design is low when compared to loading conditions which offer a larger (and safer) margin between the shakedown and limit curves.

The same study was conducted for  $R/r = 3$  under closing bending, shown in Figure 12. The trends observed for opening bending apply equally to closing bending.

### 5.3 Effect of the ratio R/r

Figure 13 presents the same results as in Figure 11 for pipe bends subject to internal pressure and opening bending but in each graph  $r/t$  is fixed and the effects of changing  $R/r$  are observed. Each geometry exhibits similar trends. The limit load curve expands with increasing  $R/r$ , and shows an increase in both the limit moment and limit pressure towards a normalised value of 1. This correlates with the expected behaviour that as  $R/r \rightarrow \infty$  the behaviour of the bend will tend towards that of a straight pipe. In terms of the shakedown limit, increasing  $R/r$  increases the normalised moment with which alternating plasticity occurs. It is also observed that the margin between the limit load and shakedown limit curves reduces with increasing  $R/r$  in all cases.

The same study was undertaken with the closing bending case, using a fixed value of  $r/t = 10$ . Figure 14 shows that the same effects and trends are observed as per the opening bending cases.

### 5.4 Comparison of Opening, Closing and Reversed Bending

Figure 15 shows a comparison between closing, opening and reversed bending for  $r/t = 10$  and  $R/r = 2, 3$  and  $5$ . The bending moment range,  $\Delta M$ , is plotted rather than the peak value of moment,  $M$ , used in previous figures. In each case the limit load surface for closing bending is larger than that for opening bending but give the same limit load for bending and pressure loading alone. Limit analysis of reversed bending is not possible due to the conflicting directions of opening and closing bending.

The shakedown limit curves show that the normalised moment at which reverse plasticity occurs does not change for any mode of bending, i.e. equation (12) applies for all three modes of bending. Closing bending has an increased ratchetting boundary over opening bending. The difference between the opening and closing bending ratchetting boundaries reduces with increasing  $R/r$ . The ratchetting boundary of reversed bending rests between that of opening and closing bending apart from the case of  $R/r=5$ , where reverse bending lies outside closing bending at the transition region between reverse plasticity and ratchetting.

Examination of the contour plots reveals that the location of the alternating plasticity mechanism does not change for opening, closing or reversed bending, and thus it is the range of the bending stress which determines the alternating plasticity boundary rather than if it is tensile or compressive.

The case of the reversed bending shakedown limit being greater than closing bending for  $R/r=5$  (Figure 15c) can be explained since both the cyclic opening bending (Figure 4a) and closing bending (Figure 4b) are equivalent to the reverse bending (Figure 4c) superimposed on a constant mean bending moment. This mean moment causes a tensile stress at the intrados for opening bending and

a compressive stress for closing bending. In the majority of the analyses performed in this paper, the addition of the stresses from the internal pressure and mean moment at the intrados is always tensile along the axis of the pipe, which results in the ratchetting mechanism beginning at the outer surface of the intrados. In the case of  $R/r=5$  for closing bending at high values of bending moment, the compressive stress from the mean moment is large enough to cause the sum of these stresses in the region to be compressive. This change to the stress causes the ratchetting mechanism to originate from the inner surface of the intrados. It is this change in ratchetting mechanism which reduces the shakedown envelope of closing bending below that of reversed bending for pressure values of  $0.45 < \left( \frac{P}{P_L^s} \right) < 0.66$ .

## **6. Internal Pressure and Cyclic Thermal Loading**

The applied temperature gradient through the wall ( $T_o=100^\circ\text{C}$  at the inner surface,  $0^\circ\text{C}$  at the outer surface) combined with the constraint that the free end expands in-plane creates the thermal stress which is used as the initial value for the cyclic stress in equation (7). The initial stress value for the constant internal pressure loading is the same as that in Figure 5a. The results presented here show the effects of  $R/r$  and  $r/t$  on the shakedown limit interaction curves. The internal pressures are normalised against equation (4) with a yield stress of 200GPa and the cyclic thermal loading,  $T$ , is normalised against the applied initial inner surface temperature  $T_o = 100^\circ\text{C}$ .

### **6.1 Temperature Dependent Yield Stress**

Figure 16 gives the shakedown boundaries for  $R/r=3$  and  $r/t=10$ , showing the difference between temperature dependent and temperature independent yield stress (temperature dependent yield values are given in Table 1). It is clear that where temperature dependency is strong, or where large temperatures are involved, it is important to consider this in the analysis. A significant reduction in the entire shakedown boundary is observed and the remainder of the results presented here therefore take temperature dependent yield stress into consideration.

### **6.2 Effect of $R/r$**

Figure 17 gives a comparison of the shakedown boundaries with changing  $R/r$  and fixed  $r/t=10$ . Also included is the shakedown boundary for a straight pipe under the same loading. It can be seen that the shape of the shakedown envelopes for the pipe bend is very similar to that of the straight pipe. As  $R/r$  of the bend increases, the shakedown envelope tends towards that of the straight pipe. This is because as the radius of the bend becomes larger with respect to the pipe radius, the effect of the

bend decreases, resulting in a lower stress concentration. When  $R/r \rightarrow \infty$  (i.e. a straight pipe) the concentration is zero. Overall, for the range of bends considered here, the reductions are relatively small when compared to a straight pipe. The most severe bend considered here,  $R/r = 2$ , has a reverse plasticity limit which is more than 90% that of the straight pipe and a ratchetting boundary which is at least 80% of the straight pipe.

### 6.3 Effect of r/t

Figure 18 shows the shakedown boundaries for fixed  $R/r = 3$  and varying values of  $r/t = 5, 10$  and  $20$ , and also that of a straight pipe with  $r/t=10$ . This shows that only very marginal changes occur to the shakedown envelope over the thickness range considered. This is primarily because the magnitude of thermal stress created is relatively independent of thickness, with only thick pipes showing an increase in thermal stress (which causes the very slightly reduced reverse plasticity boundary for  $r/t=5$  in Figure 18). Overall, the pipe thickness has little effect on the normalised shakedown limit interaction diagram (clearly the absolute values will be affected).

## **7. Conclusions**

Shakedown and limit surfaces for pipe bends covering a large range of bend characteristics are presented. Non-dimensionalising the results against limit moments and pressures for an equivalent straight pipe allows trends to be identified with changing  $R/r$ ,  $r/t$  and closing and opening bending. Based on the results presented, the following observations and design recommendations are proposed:

- The Linear Matching Method has been verified by incremental full cyclic FEA and ABAQUS Rik's analyses, showing that it gives very accurate shakedown limit and limit load envelopes.
- When subject to internal pressure and cyclic in-plane bending, the normalised moment corresponding to the reverse plasticity limit is related to  $h$  by equation (12) for all three modes of bending. The shakedown envelopes show no further trends with  $h$ ; the ratios  $R/r$  and  $r/t$  must be considered to ascertain the behaviour.
- Decreasing  $r/t$  increases the normalised cyclic bending moment corresponding to the reverse plasticity limit. Decreasing  $r/t$  also decreases the margin between the shakedown envelope (for cyclic loading) and the limit load surface (for monotonic loading). Designers must therefore take care to ensure that a sufficient margin is present to prevent an unexpected increase in the cyclic load causing plastic collapse.

- Increasing  $R/r$  increases the normalised cyclic bending moment corresponding to the reverse plasticity limit. Additionally, increasing  $R/r$  decreases the margin between the shakedown and limit surfaces, and so care should be taken to ensure sufficient margin is present.
- Opening and closing bending show no difference in the trends displayed, and all those stated above can be equally applied to either opening or closing bending.
- Direct comparison of opening and closing bending shows that closing bending gives a larger limit load surface. The normalised bending moment which causes reverse plasticity is not changed for opening, closing or reversed bending. Closing bending shows an increased ratchetting limit over opening bending, with these curves converging with increasing  $R/r$ .
- At high  $R/r$  values, closing bending may have a smaller shakedown envelope than reversed bending due to a change in the closing bending ratchetting mechanism at high values of bending moment.
- Temperature dependent yield stress is an important design consideration as significant reductions in the shakedown limit envelope can result.
- Smaller  $R/r$  ratios reduce the shakedown limit envelope when the pipe is subject to constant internal pressure and a cyclic thermal stress, but the lowest  $R/r$  considered in this paper still had more than 80% of the shakedown strength of a straight pipe.
- $r/t$  is shown to have very little impact on the shakedown limit envelope for normalised values of internal pressure and cyclic thermal stress (clearly the absolute values of these loads will change with changing  $r/t$ ).

### **Acknowledgments**

The authors gratefully acknowledge the support of the Engineering and Physical Sciences research Council of the United Kingdom, The University of Strathclyde and British Energy Generation Ltd during the course of this work. The authors would also like to thank Mr David Tipping of British Energy Generation Ltd for his advice and support.

### **References**

- [1] Bree J. Elastic-Plastic Behaviour of thin tubes Subjected to Internal Pressure and Intermittent High-Heat Fluxes with Application to Fast Nuclear Reactor Fuel Elements. *Journal of strain Analysis* 1967;2(3):226-238
- [2] Koiter WT. General theorems for elastic plastic solids. *Progress in solid mechanics*, Sneddon JN and Hill R, eds., North Holland, Amsterdam, 1960;1:167-221

- [3] Melan E. Theorie statisch unbestimmter systeme aus ideal-plastischem baustoff. Sitzungsber. d. Akad. d. Wiss., 1936;Wien 2A(145):195–218
- [4] Seshadri R. Inelastic evaluation of mechanical and structural components using the generalized local stress strain method of analysis. Nuclear Engineering and Design, 1995;153(2-3):287-303
- [5] Mackenzie D, Boyle JT, Hamilton R. The elastic compensation method for limit and shakedown analysis: a review. Trans IMechE, Journal of Strain Analysis for Engineering Design, 2000;35(3):171-188
- [6] Liu YH, Carvelli V, Maier G. Integrity assessment of defective pressurized pipelines by direct simplified methods. International Journal of Pressure Vessels and Piping, 1997;74:49–57
- [7] Chen HF, Ponter ARS. Shakedown and limit analyses for 3-D structures using the Linear Matching Method. International Journal of Pressure Vessels and Piping, 2001;78:443–451
- [8] Chen HF. Lower and upper bound shakedown analysis of structures with temperature-dependent yield stress. ASME Journal of Pressure Vessel Technology 2010;132(1):011202-1
- [9] Ainsworth RA (editor). R5: an assessment procedure for the high temperature response of structures. British Energy Generation Ltd., 2003;(3)
- [10] Calladine CR. Limit Analysis of Curved Tubes. Journal of Mechanical Engineering Science 1974;16(2):85-87
- [11] Goodall IW. Lower Bound Limit Analysis of Curved Tubes Loaded by Combined Internal Pressure and In-Plane Bending Moment. Central Electricity Generation Board (1978) Report RD/B/N4360.
- [12] Lei Y. Review of Limit Load Solutions for Defect Free Pipe Bends. British Energy Generation Ltd (2009) E/REP/BBGB/0034/GEN/08.
- [13] Abdalla F, Megahed MM, Younan MYA. Shakedown Limits of a 90 Degree Pipe Bend Using Small and Large Displacement Formulations. Journal of Pressure Vessel Technology 2007;129:287-295
- [14] Oh CS, Kim YJ, Park CY. Shakedown Limit Loads for Elbows under Internal Pressure and Cyclic In-plane Bending. International Journal of Pressure Vessels and Piping 2008;85:394-405.
- [15] ABAQUS. User's Manual Version 6.9. 2009.
- [16] British Standards Institute. Specification for "Unfired Fusion Welded Pressure Vessels". PD 5500:2006.

[17] Chen X, Gao B, Chen G. Ratcheting Study of Pressurised Elbows Subjected to Reversed In-Plane Bending. *Journal of Pressure Vessel Technology* 2006;128:525-532.

Table 1 - Temperature Dependent Yield Stress

Temperature (°C)	0	50	100	150	200	250	300	350
Yield Stress (MPa)	200	137	126	115	112	100	86	79

## **Figure Captions**

Figure 1 - Pipe Bend with Attached Straight Sections

Figure 2 - Typical Meshed FEA Model

Figure 3 - Application of Pure Bending Moment Using the DLOAD Subroutine

Figure 4 - Application of Cyclic Bending Moment During Shakedown Analysis for a) Opening Bending, b) Closing Bending and c) Reversed Bending

Figure 5 - Elastic solutions for a) Internal Pressure and b) Opening Bending

Figure 6 - Shakedown Limit and Limit Load curves for  $R/r = 2$ ,  $r/t = 5$ , Internal Pressure and Opening Bending

Figure 7 - Contour Plots of Plastic Strain to Show Failure Mechanisms of a) Alternating Plasticity at Point A and b) Ratcheting at Point B

Figure 8 - Comparison of LMM with Data from C.S. Oh et al for  $R/r=2$ ,  $r/t=10$  Subject to Internal Pressure and Opening Bending

Figure 9 - Plastic Strain Histories for Points C and B by Full Cyclic FEA

Figure 10 - Shakedown Limit Interaction Curves for  $h=0.1$  to  $h=1$ , Internal Pressure and Opening Bending

Figure 11 - Effect of changing  $r/t$  with a)  $R/r=2$ , b)  $R/r=3$  and c)  $R/r=5$ , opening bending

Figure 12 - Effect of changing  $r/t$  with fixed  $R/r=3$ , closing bending

Figure 13 - Effect of Changing  $R/r$  with a)  $r/t=5$ , b)  $r/t=10$  and c)  $r/t=20$ , opening bending

Figure 14 - Effect of changing  $R/r$  with fixed  $r/t=10$ , closing bending

Figure 15 - Comparison of Closing and Opening Bending for fixed  $r/t=10$  and a)  $R/r=2$ , b)  $R/r=3$  and c)  $R/r=5$

Figure 16 - Effect of Temperature Dependent Yield Stress,  $R/r=3$  and  $r/t=10$

Figure 17 - Effect of changing  $R/r$  with  $R/r=2, 3$  and  $5$  and Straight Pipe with fixed  $r/t=10$

Figure 18 - Effect of Changing  $r/t$  with  $r/t=5, 10$  and  $20$  with fixed  $R/r=3$  and straight pipe with  $r/t=10$

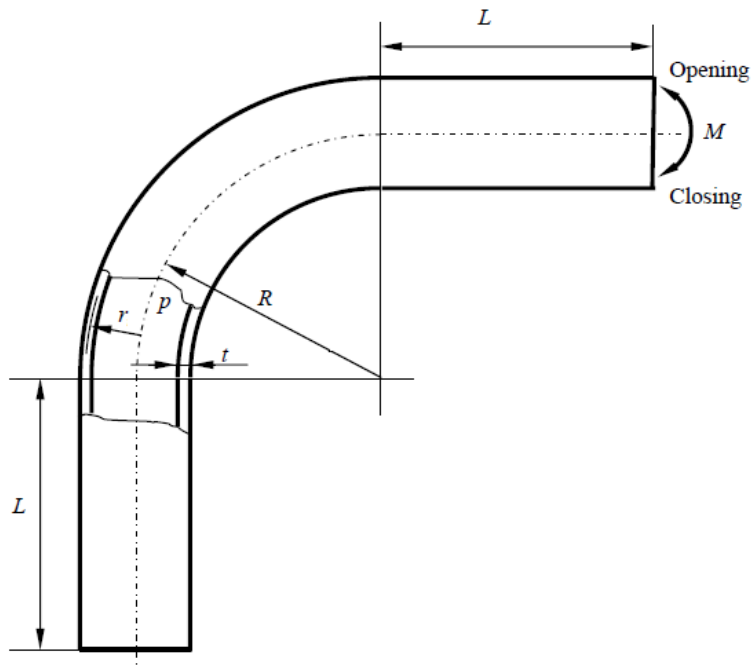


Figure 1 - Pipe Bend with Attached Straight Sections

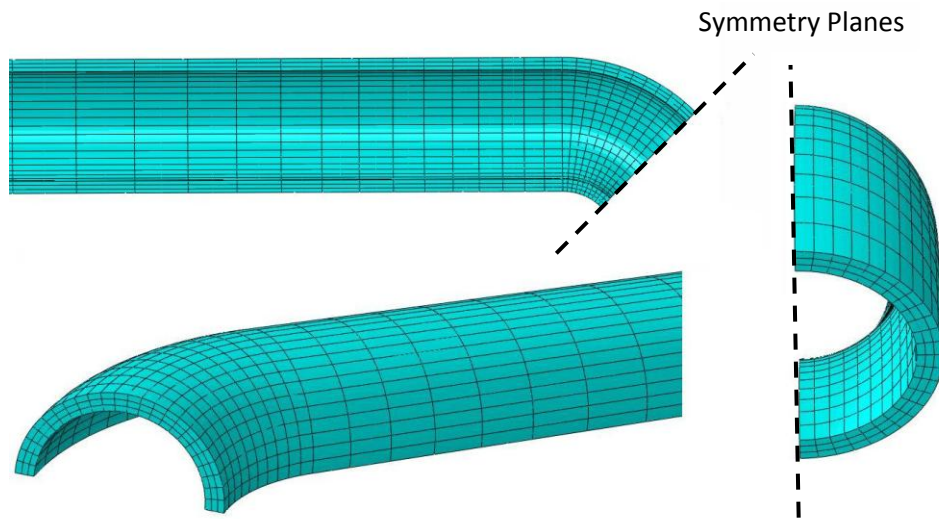


Figure 2 - Typical Meshed FEA Model

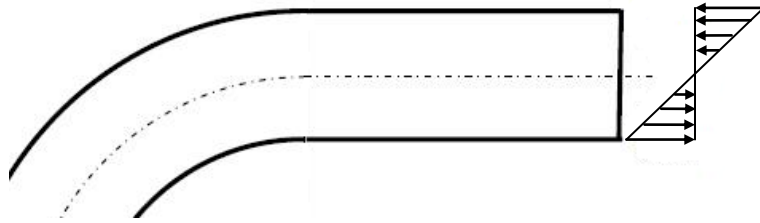


Figure 3 - Application of Pure Bending Moment Using the DLOAD Subroutine

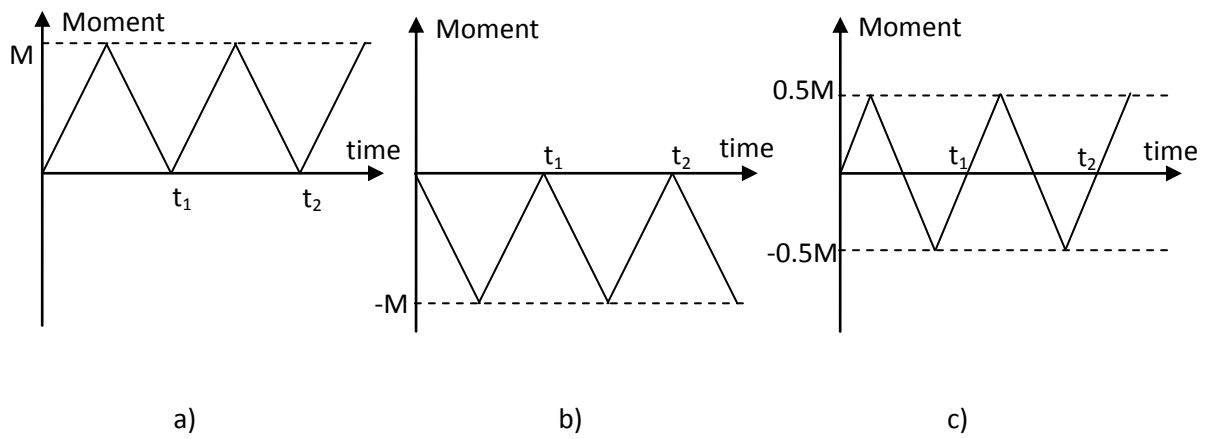


Figure 4 - Application of Cyclic Bending Moment During Shakedown Analysis for a) Opening Bending, b) Closing Bending and c) Reversed Bending

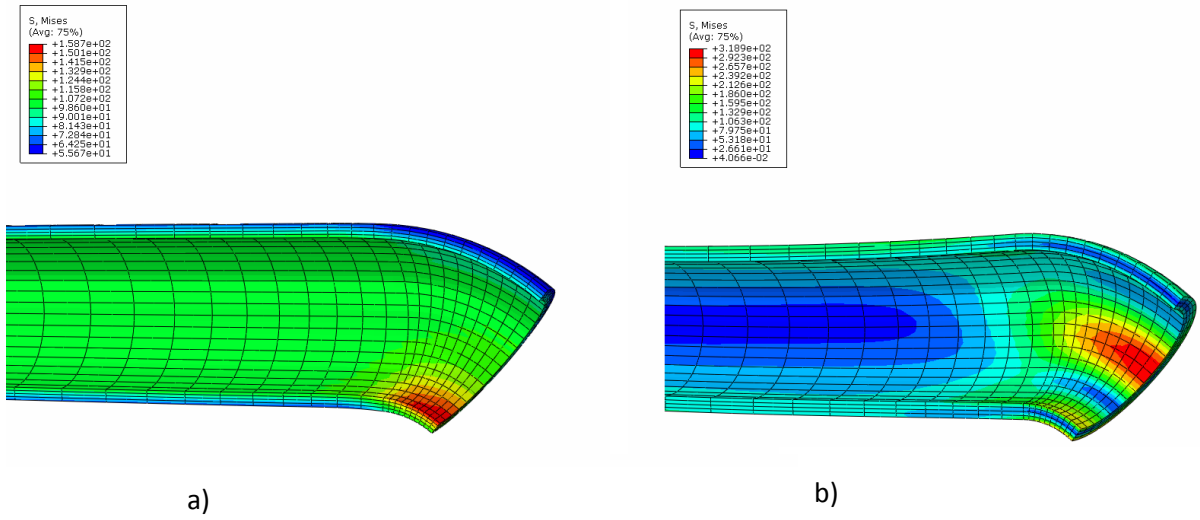


Figure 5 - Elastic solutions for a) Internal Pressure and b) Opening Bending

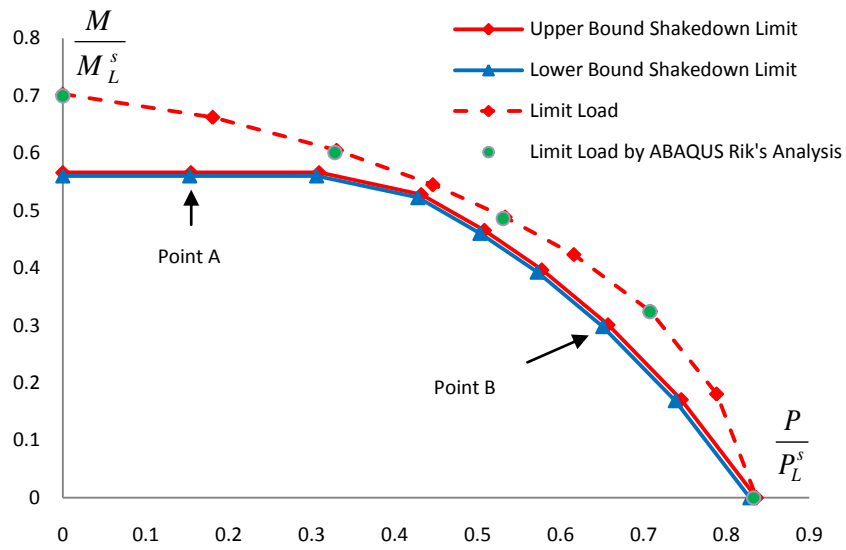


Figure 6 - Shakedown Limit and Limit Load curves for  $R/r = 2$ ,  $r/t = 5$ , Internal Pressure and Opening Bending

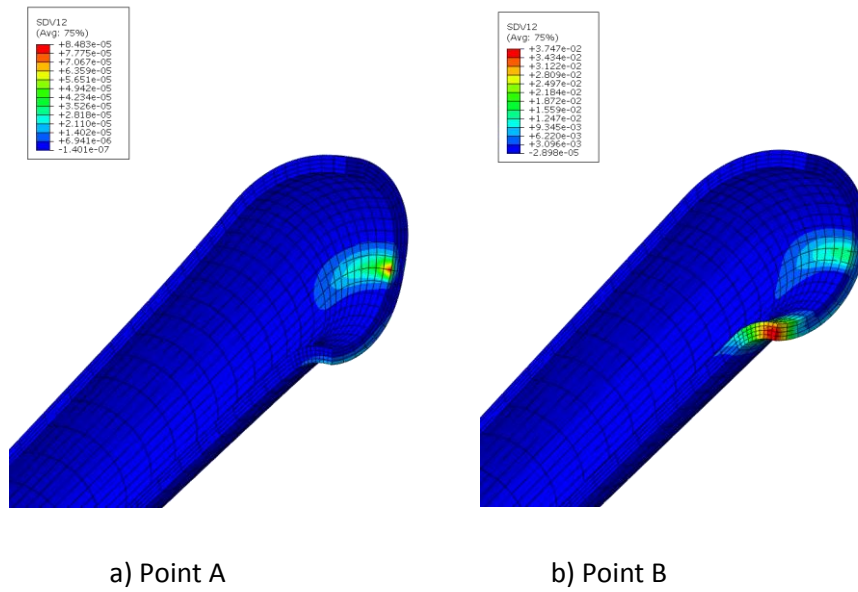


Figure 7 - Contour Plots of Plastic Strain to Show Failure Mechanisms of a) Alternating Plasticity at Point A and b) Ratcheting at Point B

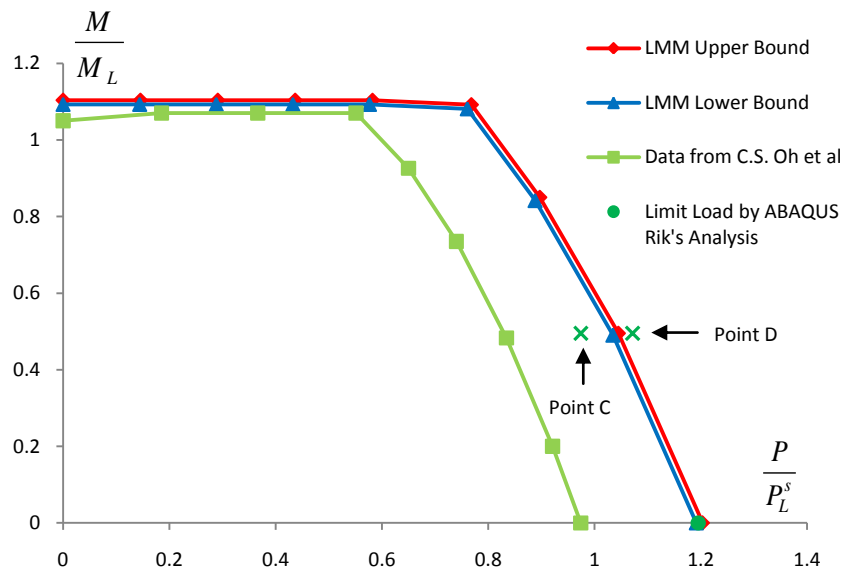


Figure 8 - Comparison of LMM with Data from C.S. Oh et al for  $R/r=2$ ,  $r/t=10$  Subject to Internal Pressure and Opening Bending

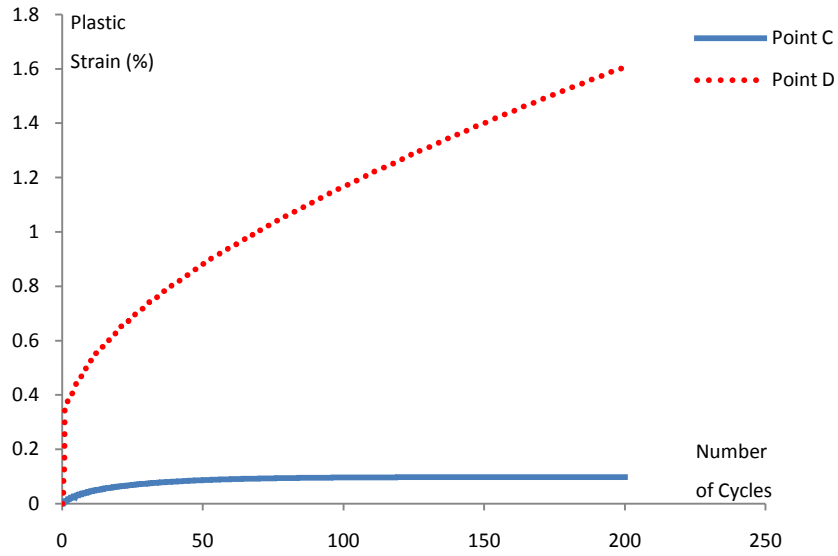


Figure 9 - Plastic Strain Histories for Points C and B by Full Cyclic FEA

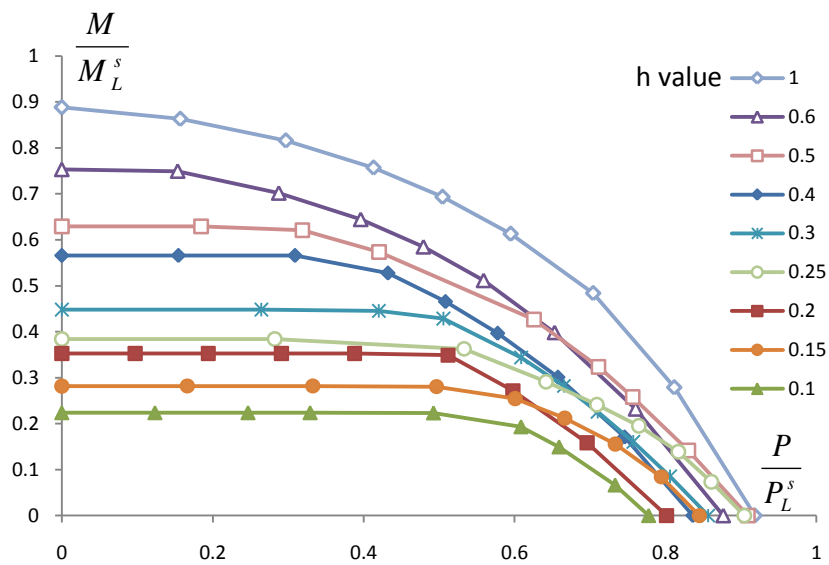
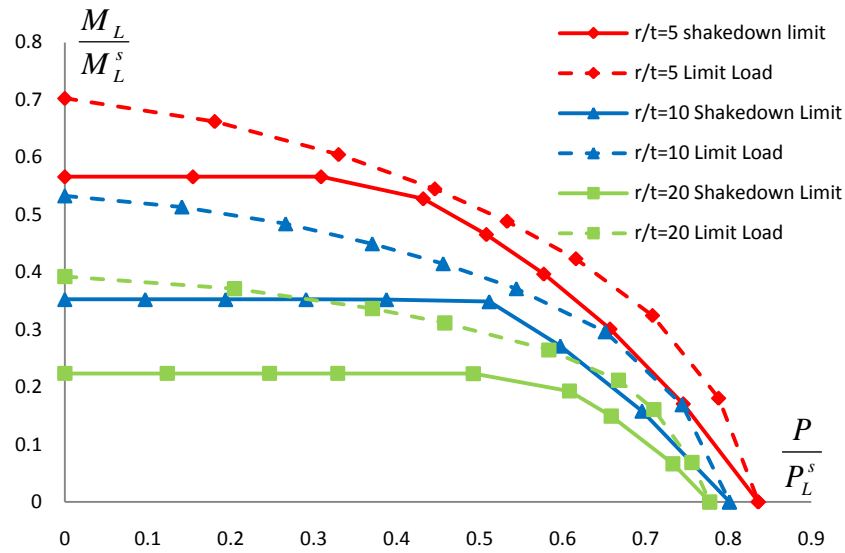
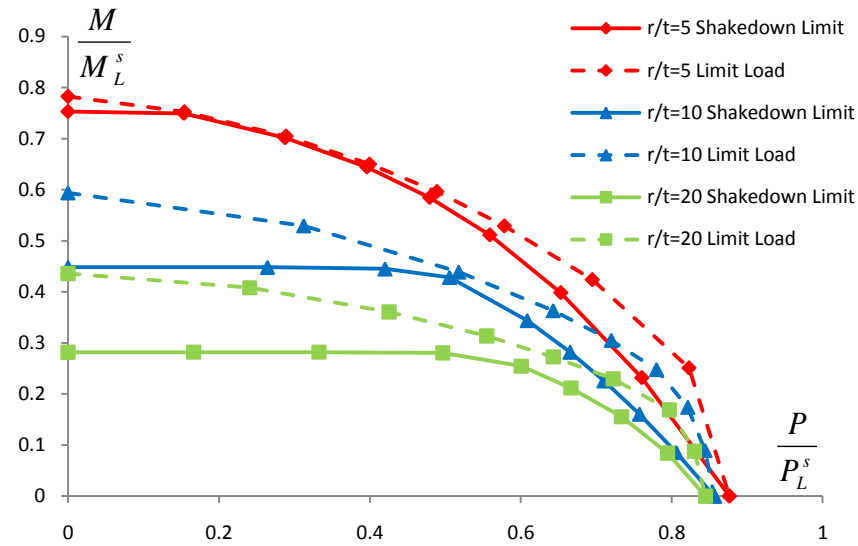


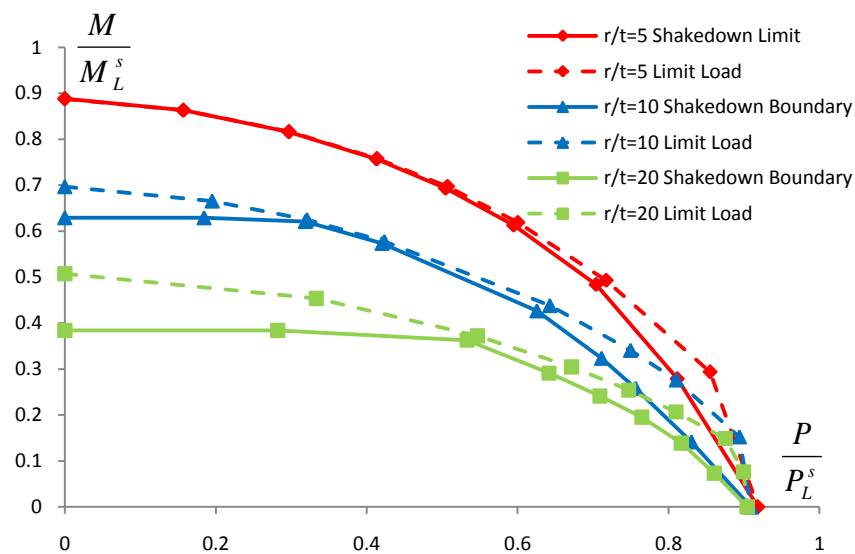
Figure 10 - Shakedown Limit Interaction Curves for  $h=0.1$  to  $h=1$ , Internal Pressure and Opening Bending



a)



b)



c)

Figure 11 - Effect of changing  $r/t$  with a)  $R/r=2$ , b)  $R/r=3$  and c)  $R/r=5$ , opening bending

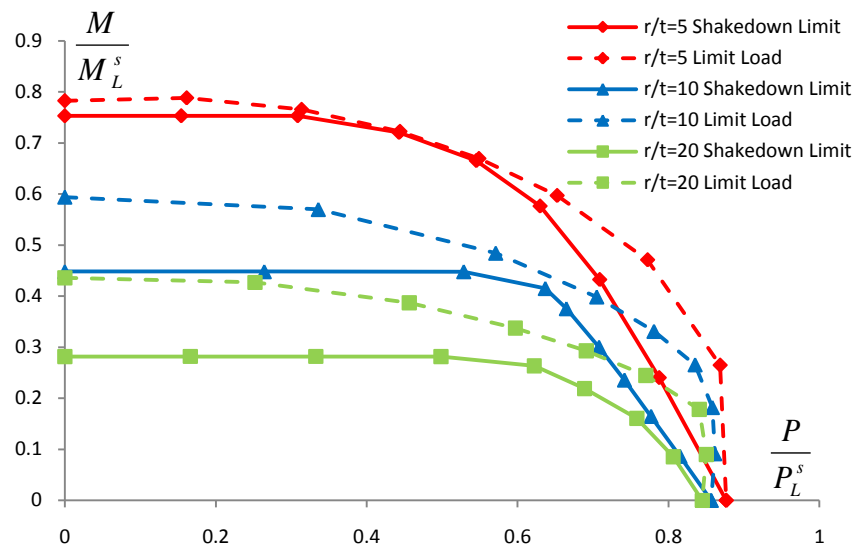
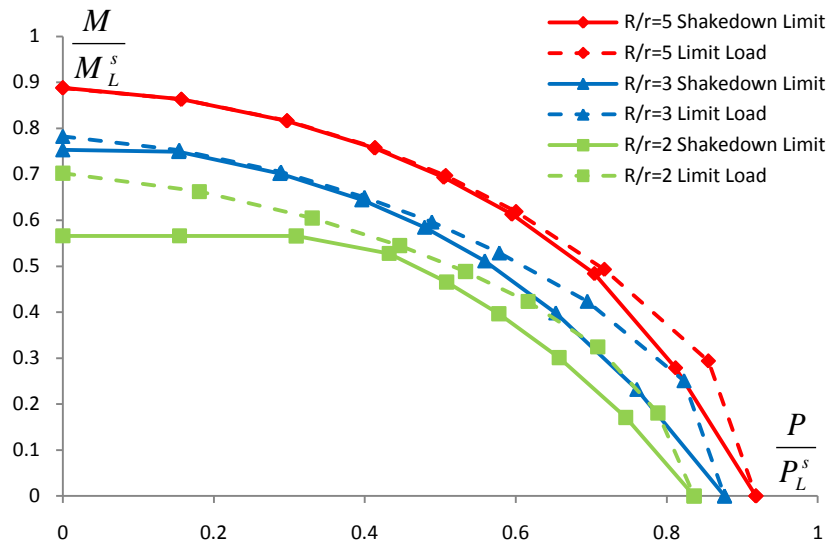
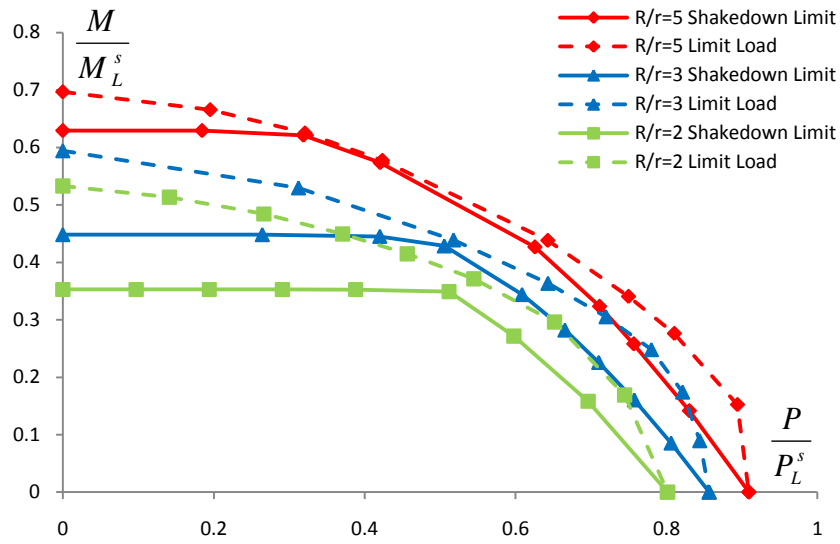


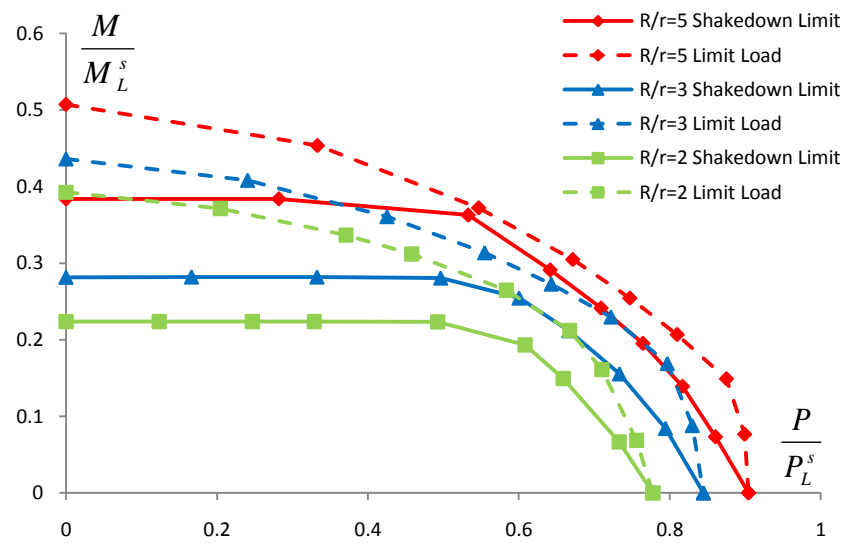
Figure 12 - Effect of changing r/t with fixed R/r=3, closing bending



a)



b)



c)

Figure 13 - Effect of Changing R/r with a) r/t=5, b) r/t=10 and c) r/t=20, opening bending

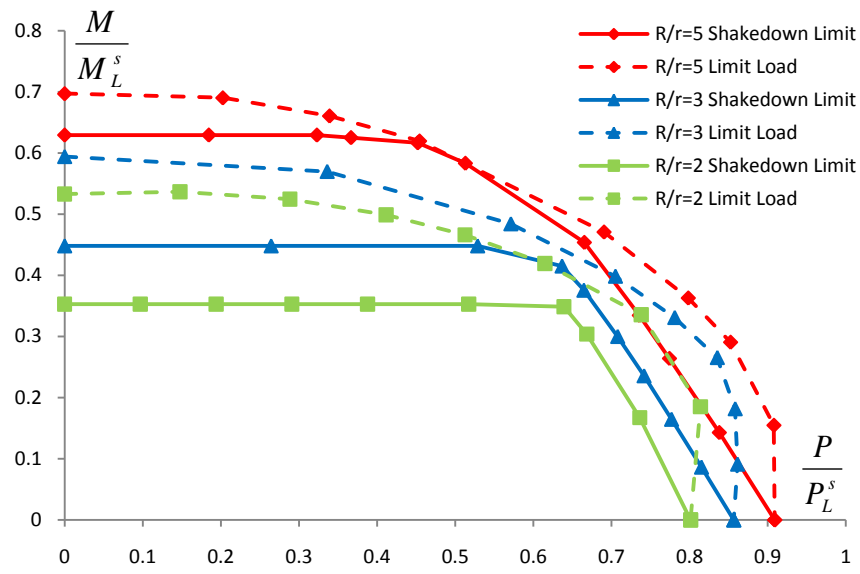
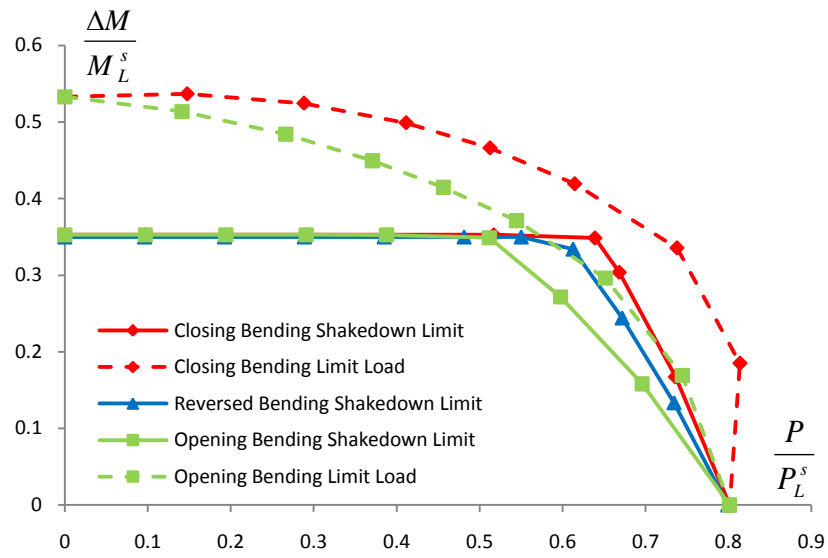
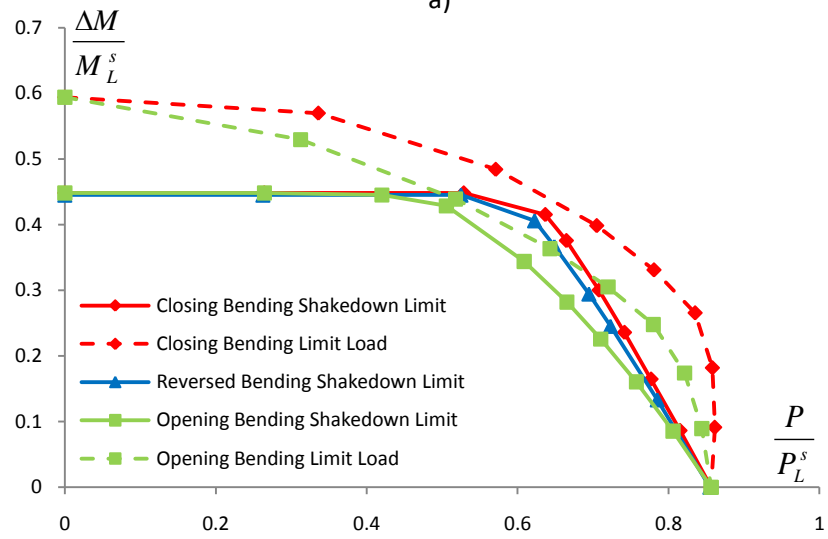


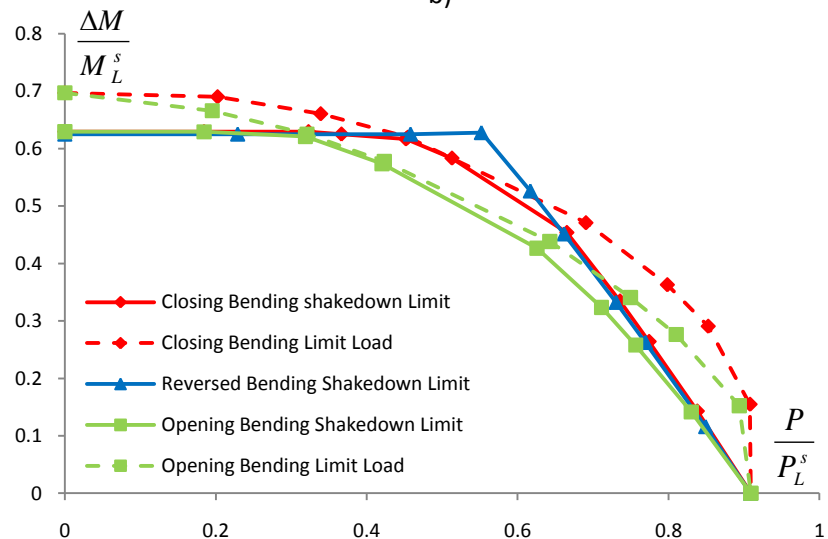
Figure 14 - Effect of changing R/r with fixed r/t=10, closing bending



a)



b)



c)

Figure 15 - Comparison of Closing and Opening Bending for fixed  $r/t=10$  and a)  $R/r=2$ , b)  $R/r=3$  and c)  $R/r=5$

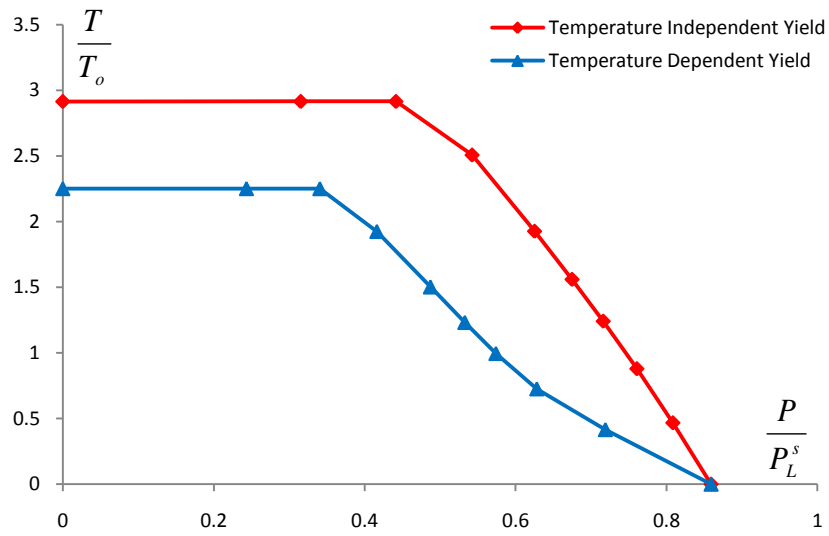


Figure 16 - Effect of Temperature Dependent Yield Stress,  $R/r=3$  and  $r/t=10$

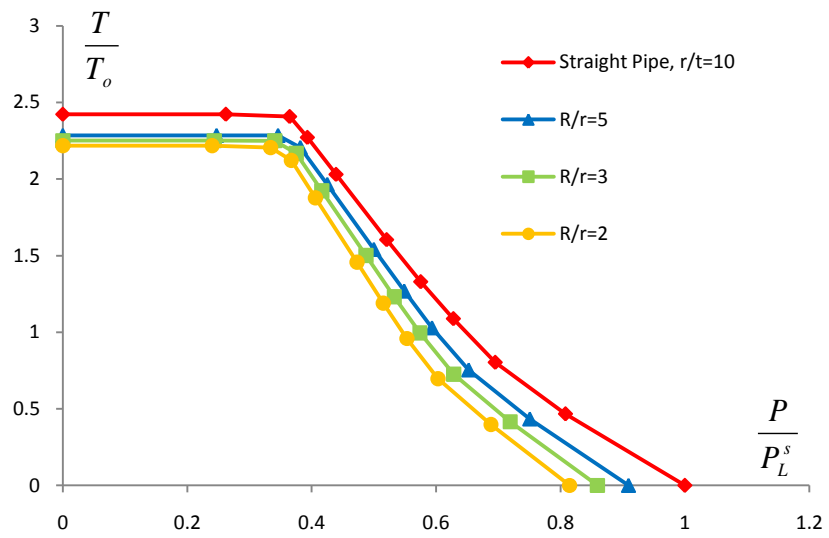


Figure 17 - Effect of changing  $R/r$  with  $R/r=2, 3$  and  $5$  and Straight Pipe with fixed  $r/t=10$

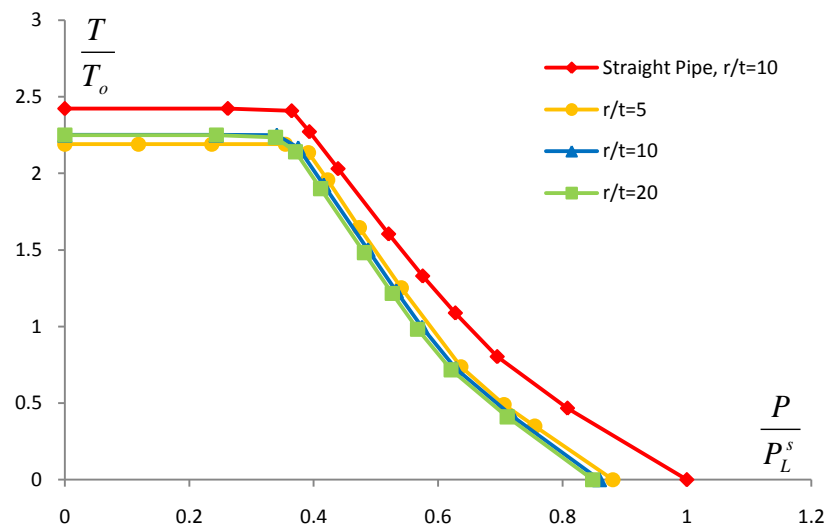


Figure 18 - Effect of Changing  $r/t$  with  $r/t=5, 10$  and  $20$  with fixed  $R/r=3$  and straight pipe with  $r/t=10$